ELSEVIER

Journal of Electroanalytical Chemistry 456 (1998) 1–12

JOURNAL OF ELECTROANALYTICAL CHEMISTRY

An exponentially expanding mesh ideally suited to the fast and efficient simulation of diffusion processes at microdisc electrodes. 1. Derivation of the mesh

D.J. Gavaghan *

Oxford University Computing Laboratory, Wolfson Building, Parks Rd., and Nuffield Deptartment of Anaesthetics, University of Oxford, Radcliffe Infirmary, Oxford, UK

Received 2 December 1996; received in revised form 21 April 1998

Abstract

The problem of numerical simulation of the current to a microdisc electrode is made difficult by the presence of a boundary singularity at the electrode edge, which causes large errors in the simulated concentration values, and consequently in the simulated flux at the electrode. We describe some simple and easily implemented strategies for deriving a refined mesh that will overcome this problem. We take as our model problem steady-state diffusion to a stationary microdisc electrode, for which the full analytic solution is known, since this allows us to demonstrate the accuracy of the numerical approximations. By making a detailed study of the causes of error in the flux calculation, we are able to show how error cancellation can be used to obtain an exponentially expanding mesh on which the flux can be evaluated to any desired degree of accuracy.

Keywords: Boundary singularities; Electrochemical control techniques; Electrode geometries

1. Introduction

In a previous paper [1], where we considered the numerical simulation of steady-state diffusion to a stationary microdisc electrode, we gave a detailed description of the effect that the boundary singularity at the electrode edge has on standard finite difference techniques. We demonstrated that practical convergence rates were much lower than predicted by theory, resulting in very inaccurate approximations for the quantity of interest, the current. Our conclusion was that it is not possible to obtain acceptably accurate simulated values for the current using standard numerical techniques on a regular spatial mesh, without making exorbitant demands on computing resources, and that accurate numerical solution to this problem is possible only if special techniques are introduced to deal with the singularity. The problems caused by such boundary singularities extend both to other electrochemical control techniques (such as chronoamperometry and in a more complex, time-dependent form, in the various types of voltammetry), and other electrode geometries (such as microband [2,3], micro-electrode arrays [4,5]), and recessed and protruding electrodes [6].

Several simulation methods have been suggested to deal with such singularities for these various electrochemical problems. Crank and Furzeland [7], Gavaghan and Rollett [8], and Galceran et al. [9] used a locally valid series expansion, Taylor et al. [10] used a mesh refinement technique based on a coordinate transformation, whilst Michael, Wightman, Amatore et al. [11–13] and Verbrugge and Baker [14] have used a coordinate transformation which effectively removes the singularity by 'folding' the radial axis at the disc edge. Evans and Gourlay [15] used a locally valid series

* Fax: +44 1865 273839; e-mail: david.gavaghan@comlab.oxford.ac.uk

0022-0728/98/$ - see front matter
PII S0022-0728(98)00239-3

expansion in calculating the flux, but made no attempt to correct the concentration values. There have also been a large number of analytic approximations for these problems (for example [17–23]).

Previous attempts at overcoming the effects of the boundary singularity by using mesh refinement (i.e. using a much finer mesh in the region of the singularity) have met with only limited success. The work of Taylor et al. [10] mentioned above appears to give accurate results, but it is not clear how to pick the most appropriate parameters in the coordinate transformation for a particular problem for which the answer is not known beforehand. Michael et al. [11], in attempting to use the exponentially expanding grid described by Heinze and Storzbach [16] for comparison with their work on conformal maps, could only achieve accuracy of 3–6%. Galceran et al. [9], using the finite element method, gave some results using both simple mesh refinement and the use of special shape functions for comparison with their work on singularity corrections but could only achieve at best 4% accuracy in reasonable computing time. Very recently, Ferrigno et al. [6], using a commercial finite element package, reported that "refining the mesh does not help deal with the conflict of boundary conditions (i.e. the boundary singularity)…(and)…divergence in the calculation of the current can be observed".

In an attempt to explain these conflicting results, and to show that when handled carefully mesh refinement can give excellent accuracy on comparatively coarse meshes, we introduce in this paper a very simple approach to mesh derivation which does not involve any transformation of coordinates. Our aim is to determine a generally applicable mesh refinement strategy that will allow us to obtain a mesh on which the flux can be simulated accurately for any electrochemical technique at a microelectrode, and in particular in this paper at a microdisc electrode. We will derive the mesh using the finite difference method since this is the easiest numerical technique to understand and implement, but the principles behind the derivation are equally applicable to the finite element method [9]. In our earlier paper [1], we described how a quick review of a large set of papers in the area yielded two levels of error as the most often quoted: 0.1% errors were usually quoted as allowing a numerical simulation method to be considered 'accurate', which was based on the accuracy achievable when solving one dimensional methods; and 1% errors were quoted as being acceptable in the simulated value of the flux when comparing with practical experimental errors. Since the primary motivation of all our numerical simulation is comparison with experimental results, we will take 1% accuracy in the simulated flux to be 'acceptable'.

One of the difficulties in determining how accurate a simulation method is for a given electrochemical problem is the lack of a 'correct' answer for most of the problems of interest, since for all problems except that of steady-state diffusion to a microdisc [24] no closed-form analytic solution for the flux exists. Throughout this paper we will therefore consider the use of our numerical methods in the solution of the steady-state problem only, since this will allow us to determine the exact nature and cause of any numerical errors.

We begin by investigating the nature of the numerical error in the simulated flux on a regular mesh, as a function of the radial distance. This allows us to show that the error is totally dominated by the error in the immediate vicinity of the singularity. We go on to devise a simple refinement strategy for reducing this component of the error, before finally devising a mesh on which, by balancing the various errors, we can achieve any desired degree of accuracy. In the accompanying papers we demonstrate that the final refined mesh that we generate in this paper will also allow us to solve the problem of chronoamperometry [28], and linear sweep voltammetry [29], both at a microdisc electrode, to the required accuracy using minimal computing resources. We have also tested this approach for other electrode geometries such as the band and recessed electrodes and found that it is equally successful at overcoming the problems caused by boundary singularities, yielding very accurate simulation results. It can also be extended very straightforwardly to multi-layer systems such as the membrane covered blood gas and enzyme sensors typical of medical applications which are our own particular area of interest [25–27].

2. The model problem

Throughout this paper, we assume that semi-infinite mass transport occurs to a disc-shaped electrode and that the electrochemical reaction

$$\mathrm{A} \pm n\mathrm{e}^- = \mathrm{B} \tag{1}$$

takes place at the disc surface. When the system is in the steady-state, axial symmetry allows mass transport to the electrode to be modelled by the cylindrical diffusion equation

$$\frac{\partial^2 u}{\partial r^2} + \frac{1}{r}\frac{\partial u}{\partial r} + \frac{\partial^2 u}{\partial z^2} = 0 \tag{2}$$

where r, z, represent the spatial coordinates. Here we solve for the normalised concentration, $u(r, z) = c(r, z)/c_0$, where c_0 is the bulk concentration of species A.

2.1. Boundary conditions

Diffusion limited transport towards the electrode and semi-infinite diffusion conditions are assumed, so the boundary conditions may be stated as:

$$z=0 \qquad r>a \qquad \frac{\partial u}{\partial z}=0$$

$$z=0 \qquad r\le a \qquad u=0$$

$$z\ge 0 \qquad r=0 \qquad \frac{\partial u}{\partial r}=0$$

$$z\to\infty \qquad r\ge 0 \qquad u=1$$

$$z\ge 0 \qquad r\to\infty \qquad u=1 \tag{3}$$

where a is the cathode (or electrode) radius. The singularity arises at $r=a$, $z=0$ due to the discontinuity in the normal derivative at the disc edge.

2.2. The current

The current, I, flowing through the disc, which is the electroanalytical response function, is given by

$$I=2\pi nFDc_0\int_0^a\left(\frac{\partial u}{\partial z}\right)_{z=0} r\ \mathrm{d}r \tag{4}$$

Here n is the number of electrons involved, F is the Faraday constant, and D is the diffusion coefficient. In order to facilitate the comparison with previous literature, we will calculate the dimensionless current, Ψ, given by

$$\Psi=I/4nFDc_0a=\frac{\pi}{2}\int_0^a\left(\frac{\partial u}{\partial z}\right)_{z=0} r\ \mathrm{d}r \tag{5}$$

2.3. The exact solution

The exact solution, $u(r,z)$, to the steady-state problem was first given by Saito [24], and in the following form by Crank and Furzeland [7]:

$$u(r,z)=\frac{c(r,z)}{c_0}-\frac{2}{\pi}\arcsin\left\{\frac{2a}{\sqrt{z^2+(a+r)^2}+\sqrt{z^2+(a-r)^2}}\right\},\quad z>0 \tag{6}$$

$$u(r,z)=0,\quad 0\le r\le a;$$

$$u(r,z)=\frac{c(r,z)}{c_0}-\frac{2}{\pi}\arcsin\frac{a}{r},\quad r>a \ \text{ on } \ z=0 \tag{7}$$

for the normalised concentration values. Differentiating Eq. (6) and setting $z=0$ we obtain

$$\frac{\partial u}{\partial z}=\frac{2}{\pi}\frac{1}{\sqrt{a^2-r^2}},\qquad 0\le r\le a \tag{8}$$

As usual we will normalise all distances to the cathode radius, allowing us to take $a=1$ in all calculations. Substituting Eq. (8) into Eq. (5) gives a non-dimensional current to the electrode of $\Psi=1$.

The exact solution Eq. (6) and Eq. (7) is valid for all $z\ge 0$, but to obtain a suitable test case for our numerical methods we will solve Eq. (2) in the finite region $[0, r_{\max}]\times[0, z_{\max}]$, and throughout most of this paper we will use values of $r_{\max}=2$ and $z_{\max}=1$. We then make use of Eq. (6) to give us the exact solution on the boundary of this region.

3. Numerical methods

To obtain a numerical solution to the electrode problem we must first discretise the solution region. Throughout this paper we will use rectangular meshes, i.e. lines of mesh points will be parallel to the coordinate axes, but need not necessarily be equally spaced. A typical example of such a mesh is shown in Fig. 1, where it can be seen that mesh lines are tightly packed around the singularity, and sparser away from the singularity[1]. We will classify the meshes using three parameters: n and m are the total number of mesh lines in the r and z-directions, respectively, and n_r is the number of points along the electrode surface. The nodes are the set of points $\{r_i, z_j\colon\ i=0\ldots n,\ j=0\ldots m\}$ which are the intersections of these mesh lines. The mesh spacings are the distances between the mesh lines and are defined by

$$h_i=r_{i+1}-r_i,\qquad i=0,\ldots,n-1 \tag{9}$$

$$k_j=z_{j+1}-z_j,\qquad j=0,\ldots,m-1 \tag{10}$$

We will therefore seek an approximate solution $U_{i,j}$ to the exact concentration $u(r_i z_j)$ at each point in the mesh. In the appendix we give a description of how this simple method of defining the mesh can be used in a very straightforward manner to obtain the necessary finite difference approximations.

3.1. Deriving a suitably refined mesh

We will use three different refinement strategies, starting with the simplest possible, i.e. successively halving the mesh spacing on a coarse, regular, square mesh, moving on to refinement only in the immediate vicinity of the singularity but with regular spacing elsewhere, and finally using refinement around the singularity and an expanding mesh away from the singularity. Each successive strategy will give information about the nature of the error in the simulated flux as a function of the mesh and the mesh spacing, which will then be used to devise the succeeding strategy.

[1] This type of mesh is superficially similar to that obtained by Taylor et al. [10] using a coordinate transformation. However, the approach described here achieves greater flexibility and transparency, as we will show in a later paper where we will compare the various approaches used to date for two dimensional problems.

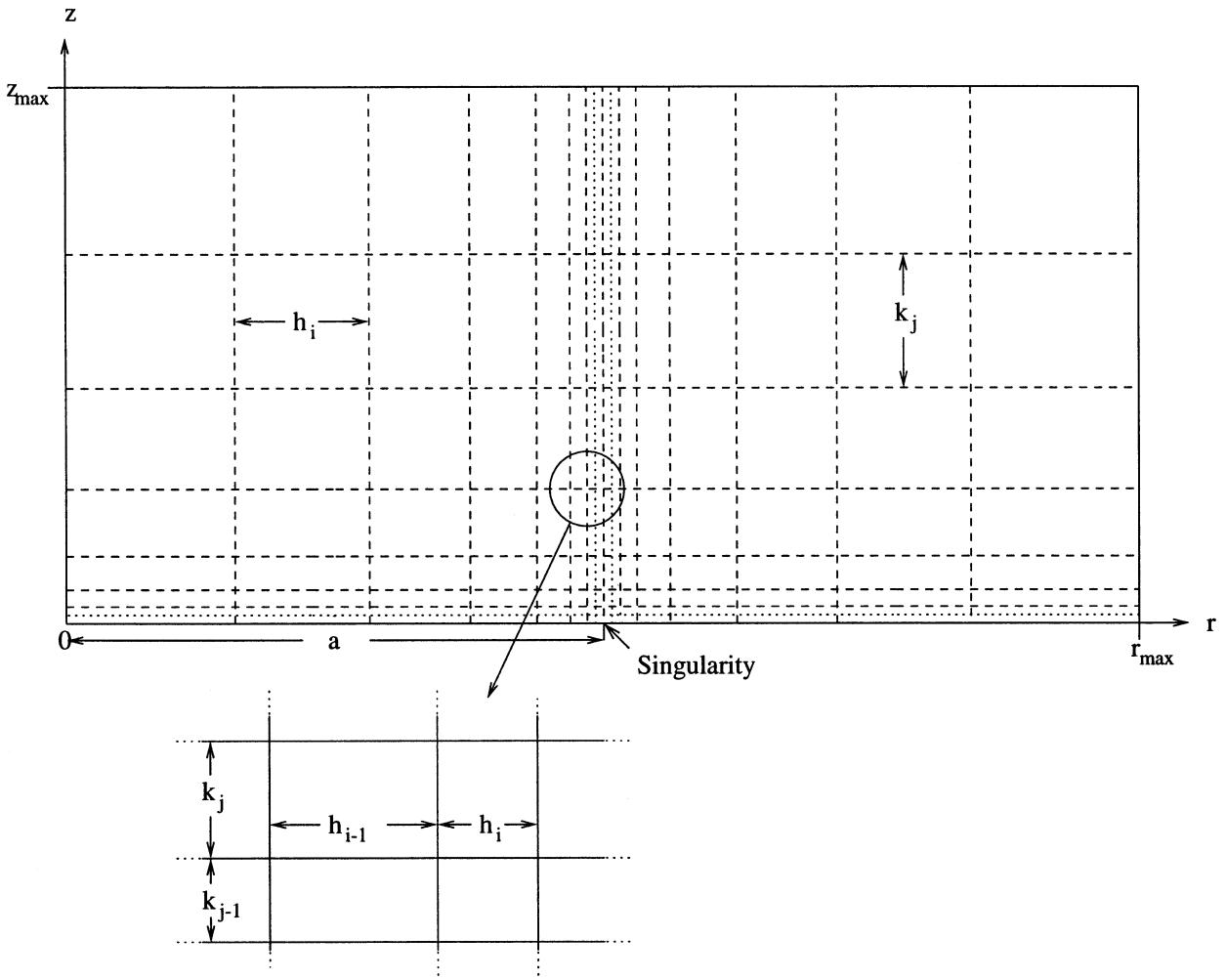

Fig. 1. A typical example of a mesh suitable for electrode problems, with mesh lines tightly packed around the singularity, and sparser away from the singularity.

3.2. Generalised second order finite differences

Throughout this paper we will use finite differences to approximate the partial differential Eq. (2) which are derived using the Taylor expansion (see Chapter 3 of Britz [33]). On a regularly spaced square mesh, with mesh spacing h, this gives the familiar central difference approximations, for example

$$u_{rr} = \frac{\partial^2 u}{\partial r^2} \approx \frac{U_{i+1,j} - 2U_{i,j} + U_{i-1,j}}{h^2}, \tag{11}$$

with the error in this approximation being proportional to h^2. On a general mesh, the corresponding mesh points are separated by spacings h_{i-1}, h_i in the r-direction and k_{j-1}, k_j in the z-direction, as shown in Fig. 1. Again using Taylor expansions, we show in the appendix how to derive the generalised second order differences as

$$u_{rr} \approx \frac{2(h_{i-1}U_{i+1,j} - (h_{i-1} - h_i)U_{i,j} + h_i U_{i-1,j})}{h_{i-1}h_i(h_{i-1} + h_i)}, \tag{12}$$

with a similar expression for u_{zz}, and for u_r we obtain

$$u_r \approx \frac{(h_{i-1}^2 U_{i+1,j} - (h_{i-1}^2 - h_i^2)U_{i,j} + h_i^2 U_{i-1,j})}{h_{i-1}h_i(h_{i-1} + h_i)}. \tag{13}$$

3.3. Neumann boundary conditions

Along $r = 0$ and on $z = 0$ for $r > 1$, we have derivative or Neumann boundary conditions. We make use of the Maclaurin expansion of $\partial u/\partial r$ on $r = 0$ to get $\partial u/\partial r = \partial^2 u/\partial r^2$, so that Eq. (2) becomes $2\partial^2 u/\partial r^2 + \partial^2 u/\partial z^2 = 0$, which is used with the conventional introduction of a 'fictitious' [30] mesh line at $i = -1$ to give $U_{-1,j} = U_{1,j}$. Combining these results with Eq. (12) gives

$$u_{rr} \approx \frac{4U_{1,j} - 4U_{0,j}}{h_0^2}, \tag{14}$$

as the second order finite difference operator along $r = 0$.

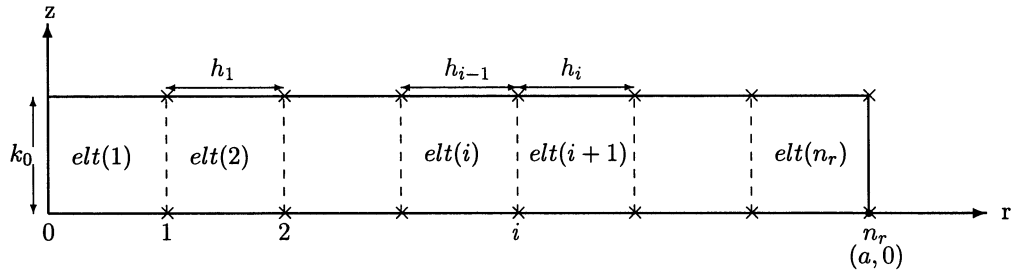

Fig. 2. The n_r sub-elements of the mesh covering the electrode surface used in calculating the flux to the electrode.

Along $z=0$ for $r>1$, we have again used Taylor expansions (see appendix) to obtain a one sided second order finite difference to u_z as

$$u_z \approx -\left(\frac{k_0^2 U_{i,2} - (k_0+k_1)^2 U_{i,1} + k_1(k_1+2k_0)U_{i,0}}{k_0 k_1 (k_0+k_1)}\right) \tag{15}$$

where k_0 and k_1 are the first two mesh spacings in the z-direction.

3.4. Dirichlet boundary conditions

On all other boundaries we have Dirichlet conditions which will be imposed using

$$\begin{aligned} U_{i,0} &= 0 && i=0,\ldots,n_r \\ U_{n,j} &= u(r_{\max}, z_j) && j=1,\ldots,m-1 \\ U_{i,m} &= u(r_i, z_{\max}) && i=0,\ldots,n-1 \end{aligned} \tag{16}$$

where $u(r,z)$ is the analytic solution given by Eq. (6). This use of the analytic solution to replace the boundary conditions 'at infinity' is rather unsatisfactory, since for the electrochemical problems of practical interest we do not know the exact analytic solution. In the accompanying papers where we consider time-dependent problems, we will replace this boundary condition by one which assumes bulk concentration at a sufficient distance from the electrode. However, initially we will find it extremely useful to be able to investigate the various mesh refinement strategies on the restricted region using the boundary conditions given by Eq. (16), and we give a brief description of its effect in Section 4.5.

3.5. Numerical solution of the finite difference equations

The various finite difference approximations described above form a linear system of equations relating the concentration values at the interior and boundary nodes. In our earlier paper [1] we described how to solve such a system using a very simple iterative method (the SOR method of Southwell [31]). However, it is also possible to express the system in matrix form and obtain the solution by direct inversion of the matrix, that is, we solve

$$A\mathbf{u} = \mathbf{d} \qquad \text{to obtain} \qquad \mathbf{u} = A^{-1}\mathbf{d} \tag{17}$$

for $\mathbf{u}$ the vector of $n(m-1)$ unknown concentration values, where A is an $n(m-1)\times n(m-1)$ matrix, and $\mathbf{d}$ an $n(m-1)$ vector containing information about the Dirichlet boundary conditions. All of the results quoted in this paper are obtained by this matrix inversion method, making use of routines F07BDF and F07BEF of the NAG Fortran Subroutine Library [32], which utilise the banded structure of the matrix.

3.6. Calculation of the flux

The quantity of interest in electrochemical experiments is the current, or equivalently, the nondimensional flux defined by Eq. (5). Our refinement strategy is therefore aimed at obtaining an acceptably accurate simulated value of the flux without making exorbitant demands in terms of computing resources. It will prove particularly useful when devising the refinement strategies, to consider the flux into each sub element of the mesh covering the electrode surface, as illustrated in Fig. 2. We can obtain the exact flux to each of these sub elements using Eqs. (5) and (8) (setting both $a=1$ and $c_0=1$) to give

$$\Psi_{\mathrm{elt}(i)} = \int_{r_{i-1}}^{r_i} \frac{r}{\sqrt{1-r^2}}\,\mathrm{d}r = \sqrt{1-r_{i-1}^2} - \sqrt{1-r_i^2} \qquad i=1,\ldots,n_r \tag{18}$$

In our earlier paper [1], we demonstrated that the most appropriate finite difference approximation to use in calculating the flux to the electrode surface is the 3-point approximation. On a general mesh this is given by (see Eq. (15) above)

$$\left(\frac{\partial u}{\partial z}\right)_{z=0} \approx \phi_i^z = -\frac{k_0^2 U_{i,2} - (k_0+k_1)^2 U_{i,1}}{k_0 k_1 (k_0+k_1)}. \tag{19}$$

The flux into each sub element is then approximated by numerical integration of Eq. (5) using the trapezium rule, which is also second order, and is the most economical way to perform this calculation [1]. For each element this gives

$$\Psi_{\mathrm{elt}(i)} \approx \frac{\pi}{2}\left(\frac{h_{i-1}}{2}(r_{i-1}\phi^{z}_{i-1} + r_i\phi^{z}_{i})\right) \quad i = 1,\ldots,n_r \qquad (20)$$

and the total flux is given by the sum over all elements on the electrode. In particular it will prove useful to compare the flux to the electrode in the final element, $\Psi_{\mathrm{elt}(n_r)}$ with that over the rest of the inner part of the electrode surface, and we therefore define

$$\Psi_{\mathrm{inner}} = \sum_{i=1}^{n_r-1} \Psi_{\mathrm{elt}(i)} \qquad (21)$$

$$\Psi_{\mathrm{last}} = \Psi_{\mathrm{elt}(n_r)}, \qquad (22)$$

and the corresponding errors, E_{inner}, and E_{last}, are defined as the difference between these simulated values and the exact values from Eq. (18).

4. The mesh refinement strategies

4.1. Aims of the refinement

As we stated in the introduction, our aim in introducing mesh refinement is to obtain a value of the simulated flux that is accurate to 1% on a mesh that is sufficiently coarse that the computing demands are reasonable. However, it is not simply our aim to find a mesh on which we can solve the steady-state problem to this accuracy, we will demonstrate in the accompanying and later papers that such a mesh will also give very accurate answers for a variety of electrochemical simulation problems at microdisc electrodes. Our approach in the following sections will be directed primarily towards this wider goal.

4.2. Strategy 1: The square mesh

The simplest possible refinement strategy is to use a square mesh with $h_i = k_j = h$, say, for all i, j, as illustrated in the upper mesh of Fig. 3. Since we are solving on the restricted region $[0, 2] \times [0, 1]$ we will have $n = 2m = 2n_r$ on all meshes. Table 1 gives the results of this refinement strategy for the simulated flux starting with $n_r = 2$ (so that $h = 1/2$) and successively halving h five times until $n_r = 64$, and $h = 1/64$. We pointed out several of the features that are evident in Table 1 in our earlier paper [1], to which the reader is referred for a more detailed discussion of their implications. Since these features will be used throughout the rest of the paper in devising successive mesh refinement strategies, we will list the most important of them here:

1. The error in the total flux to the electrode becomes increasingly dominated by the error in the last element which is immediately adjacent to the singularity, so that by the 128×64 mesh, the error from the inner 63 elements covering the electrode is just $+0.16\%$ of the total flux over the whole electrode, whilst that due to the 64th and last element is -6.7%.

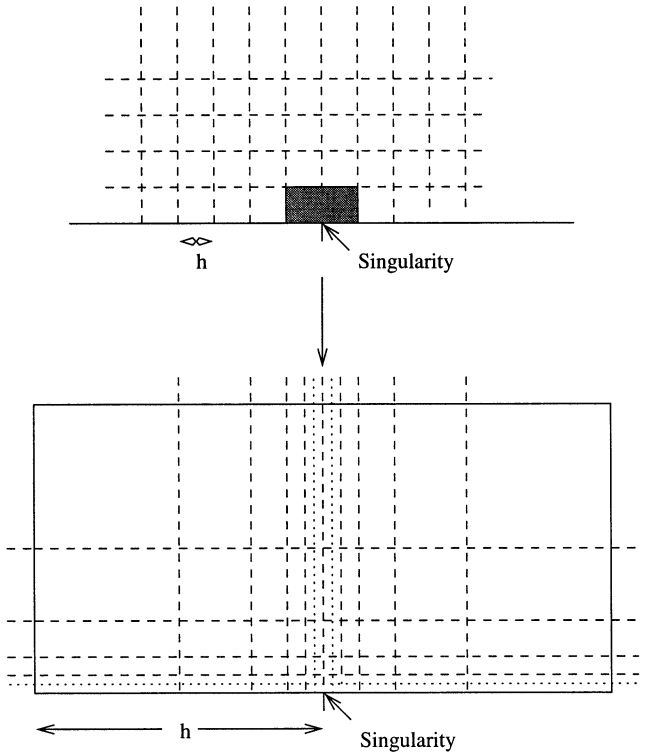

Fig. 3. The upper mesh is the simple regular mesh used in Strategy 1. This is then refined in the shaded region adjacent to the singularity as shown in the lower mesh to obtain Strategy 2, and all mesh lines are extended out to the boundary in both directions (as in Fig. 1).

Table 1
The results of mesh refinement on a square mesh

n_r	Mesh ($n \times m$)	E_{inner}	E_{last}	Ratio	Flux (Ψ)	Error	Ratio
2	4×2	$+0.3938$	$+0.7148$	—	2.109	1.109	—
4	8×4	$+1.081 \times 10^{-2}$	-0.2586 (39.1%)	1.38	0.7522	-0.2478	1.38
8	16×8	$+7.963 \times 10^{-3}$	-0.1872 (38.7%)	1.40	0.8207	-0.1793	1.39
16	32×16	$+4.909 \times 10^{-3}$	-0.1338 (38.5%)	1.40	0.8711	-0.1289	1.40
32	64×32	$+2.868 \times 10^{-3}$	-0.0951 (38.3%)	1.41	0.9078	-0.0912	1.40
64	128×64	$+1.653 \times 10^{-3}$	-0.0674 (38.3%)		0.9342	-0.0658	

The value in the Ratio columns gives the ratio of the error in that row, with that of the next row. The error in the flux in the last element on the electrode is also shown as a percentage of its exact value.

2. The ratio of the errors in the last box on successive meshes is $\sqrt{2}$ implying that the rate of convergence in this element is $h^{1/2}$, rather than the h^2 that we might expect from convergence theory for second order finite differences. Since this error eventually dominates that for the total flux, the convergence rate for the total flux can also be seen to be tending to $h^{1/2}$.
3. The error in the last element is always negative, whilst that in each of the other elements is always positive. We therefore get a small amount of error cancellation (see Britz [33]).
4. The percentage error in the flux in the last element (given in brackets in Table 1) becomes constant. This is simply a further reflection of the $h^{1/2}$ convergence: from Eq. (18) it can be seen that the exact flux to the last element is also proportional to h^2.

Knowing the exact rate of convergence in the last element allows us to calculate how many mesh points covering the electrode would be required to give a value of the simulated flux accurate to 1%: successively halving the mesh spacing h a further six times would reduce E_{last} by a factor of 8, giving an error of about 0.85%. However, this would require about 4000 nodes along the electrode and a mesh with about 30 million unknowns, which is not feasible in a finite computing time.

4.3. Strategy 2: Refinement in the vicinity of the singularity

From the observations made from Strategy 1, it seems clear that if we simply add in additional points close to the singularity, i.e. refine the mesh, we should obtain a more accurate value for the flux. The simplest way to do this is to begin with a regular square mesh with n_r points along the electrode giving spacing $h = h_{\text{inner}} = 1/n_r$. We then successively halve[2] the distance between the final mesh point at the singularity and those immediately adjacent to it in both the r and z-directions, as illustrated in the lower mesh shown in Fig. 3. If we half this distance l_r, l_z times in the r and z-directions, respectively, then the mesh spacings will be given by

$$h_i = \begin{cases} h & \text{for} \quad i = 0,\ldots,n_r - 2 \\ h_{i-1}/2 & \text{for} \quad i = n_r - 1,\ldots,n_r + l_r - 2 \\ h_{n_r + l_r - 2} & \text{for} \quad i = n_r + l_r - 1 \\ h_{2(n_r + l_r) - 1 - i} & \text{for} \quad i = n_r + l_r,\ldots,2(n_r + l_r) - 1 \end{cases}$$

[2] It is, of course, not necessary to choose to halve the mesh: any refinement procedure for which we can define the mesh spacings is acceptable, and the computer program that we have used to solve this problem allows any fractional ratio between 0 and 1. We do not give any results here for ratios other than one half since this value provides all the information needed to move on to the third, and most computationally economical, refinement strategy.

Table 2
The results of successively halving the mesh spacing in the redirection only immediately adjacent to the singularity (see Fig. 3)

l_r	l_z	h_{inner}	h_{last}	E_{inner}	E_{last}	Flux (Ψ)
0	1	0.25	2^{-2}	+0.0108	−0.2586	0.7522
1	1	0.25	2^{-3}	+0.0280	−0.2250	0.8030
3	1	0.25	2^{-5}	+0.0252	−0.1649	0.8602
7	1	0.25	2^{-9}	−0.0615	−0.0568	0.8817
11	1	0.25	2^{-13}	−0.1016	−0.0153	0.8831
12	1	0.25	2^{-14}	−0.1059	−0.0109	0.8832
13	1	0.25	2^{-15}	−0.1090	−0.0077	0.8832
14	1	0.25	2^{-16}	−0.1113	−0.0055	0.8832

$$k_j = \begin{cases} h/2^{l_z} & \text{for} \quad j = 0, 1 \\ 2k_{j-1} & \text{for} \quad j = 2,\ldots,l_z \\ h & \text{for} \quad j = l_z + 1,\ldots,l_z + n_r. \end{cases} \tag{23}$$

which can then be used to calculate the appropriate finite differences as described earlier.

We will demonstrate the effect of this refinement strategy in three stages. We will begin with a very coarse regular mesh[3] using $h = h_{\text{inner}} = 4$, $n_r = 4$, and we will first refine in the v-direction only as shown in Table 2. As can be seen, after halving the mesh spacing 12 times, the overall flux to the electrode no longer changes, although the error continues to move from the last element (where the error continues to decay at the rate $h^{1/2}$) to the inner part of the electrode. It is worth noting that for $l_r = 12$ the error in the last element is about 1% of the total flux. We therefore take this mesh as the starting point of the second stage of the refinement: successively halving the mesh spacing in the z-direction immediately above the electrode surface. The results are shown in Table 3. By the twelfth level of refinement the error in the total flux is dominated by the inner error which is positive and totals about +3% whilst that in the last element is negative and is less than 0.5%.

Table 3
The results of successively halving the mesh spacing in the z-direction only immediately above the electrode (see Fig. 3)

l_z	l_r	h_{inner}	h_1	E_{inner}	E_{last}	Flux (Ψ)
0	12	0.25	2^{-2}	−0.1059	−0.0109	0.8832
1	12	0.25	2^{-3}	−0.0333	−0.0108	0.9559
3	12	0.25	2^{-5}	−0.0230	−0.0105	1.012
7	12	0.25	2^{-9}	+0.3835	−0.0090	1.029
11	12	0.25	2^{-13}	+0.0329	–0.0049	1.028
12	12	0.25	2^{-14}	+0.0314	−0.0041	1.027

h_1 is the mesh spacing immediately above the electrode.

[3] From Table 1 it can be seen that even on this mesh the error in the flux is dominated by the singularity.

Table 4
The results of refining the underlying mesh, so that the spacing h_{inner} is successively halved

h_{inner}	$h_1 = h_{\text{last}}$	n_{inner}	$l_z \times l_r$	E_{inner}	E_{last}	Flux (Ψ)
0.5	2^{-14}	1	13×13	0.0496	−0.0040	1.046
0.25	2^{-14}	3	12×12	+0.0314	−0.0041	1.027
0.125	2^{-14}	7	11×11	+0.0162	−0.0042	1.012
0.0625	2^{-14}	15	10×10	+0.0078	−0.0042	1.004
0.03125	2^{-14}	31	9×9	+0.0037	−0.0042	0.9995

n_{inner} is the number of mesh points covering the inner part of the electrode surface.

These observations suggest that the final step is to refine the original mesh away from the singularity, to reduce the inner error to less than 0.5% so that the total error will be less than our target of 1%. Of course, if we can do this in such a way that this inner error remains positive, error cancellation will give us a value of the total flux that is much more accurate than 1%. We do this by successively halving the underlying mesh spacing h as shown in Table 4, whilst keeping the level of refinement immediately adjacent to the singularity constant. As anticipated, the error in the last element remains roughly constant, whilst the inner error decays (at roughly order h_{inner}), but remains positive, so that we get error cancellation, giving a flux on our finest mesh being accurate to 0.05%. Any further refinement would need to be carried out on both the inner part of the electrode and in the vicinity of the singularity, and as a rough guide we would expect that we could halve the total error by halving h_{inner} and quartering h_{last}.

The final mesh in Table 4 has 40 mesh points along the electrode surface and the total mesh covering the restricted solution region is 80×40, that is, we have achieved our objective of better than 1% accuracy on a fairly coarse mesh. However, this approach has several drawbacks: firstly, as shown by the full line in Fig. 4, the error in the flux is very small close to the axis of symmetry, but increases rapidly close to the singularity; secondly, the mesh requires the definition of several parameters which can each be varied and which will each cause changes in the error in the calculated flux; thirdly, and most importantly, whilst this mesh is satisfactory for the restricted region used so far, for a problem where we do not know the exact solution, we will have to solve over a much larger region, and we will wish to use an expanding mesh away from the singularity or the mesh will be prohibitively large (e.g. typically in a chronoamperometry experiment we may require a solution in the region $[0, 40] \times [0, 40]$ which would correspond to a mesh with around 1300 nodes in each direction using this technique).

4.4. Strategy 3: The expanding mesh

However, whilst Strategy 2 may not be the most appropriate, we can again use the information provided by Tables 2–4 to suggest improvements. We have shown that the error in the last element decays with order $h^{1/2}$, and that this rate of decay persists when we refine locally. Since our overall requirement is 1% accuracy, it would therefore seem sensible to choose the mesh spacing immediately adjacent to the singularity (h_{last}) to give 0.5% error into the last element, and then gradually increase the mesh spacing away from the singularity in a way that gives a fairly uniform flux error distribution over the inner part of the electrode, but with a total inner error of 0.5%. This may at first seem an odd procedure: we wish to obtain 1% error overall, but we are choosing to limit two errors of opposite signs to just 0.5%, so that clearly, thanks to error cancellation, we will greatly exceed our target accuracy. The reason for doing this is that this simple test problem is not our primary interest, our main interest is the simulation of more complex electrochemical problems, such as time-dependent chronoamperometry and voltammetry dealt with in the accompanying papers. Our assumption in choosing to limit both the inner and outer errors to less than 0.5% is that

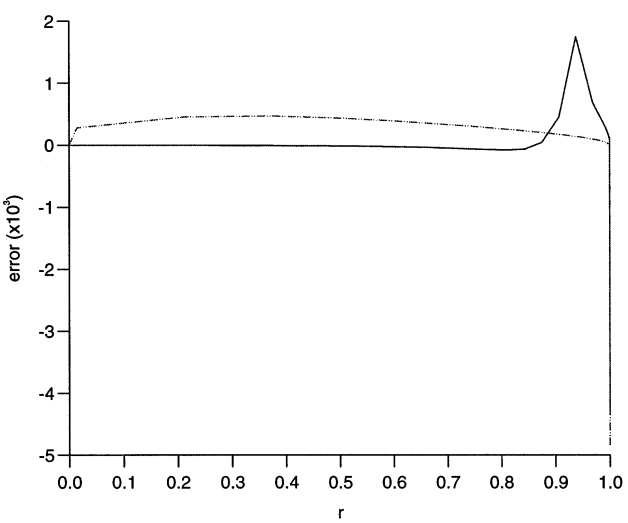

Fig. 4. Plot of the error in the simulated flux plotted as a function of the radial distance r. The full line shows the error obtained using the finest mesh ($n_{\text{inner}} = 31$) from Table 4, whilst the dashed line shows the error obtained using the fine mesh shown in Fig. 5 with $h_{\text{last}} = 8.0 \times 10^{-4}$ and $f = 1.25$.

whilst we expect the errors in simulating these more complex problems to be of similar absolute size, it is unlikely that they will balance in an identical fashion to those for the steady-state problem, since the transport processes being modelled differ. Obviously, we do hope that some of the error cancellation will carry through to these problems, but by choosing to limit each to 0.5%, we should ensure an overall error of less than 1% even if no error cancellation takes place. In practice, as we show in the accompanying paper we are able to obtain much better than 1% error in all cases considered.

We can achieve the first of these aims using the information in Table 4. We know that the error decays like $h^{1/2}$ in the last element, so that $E_{\text{last}} = 0.0042 \approx Ch^{1/2}$ for some constant C. Since $h = 2^{-14}$ in this element, we have that $C \approx 0.0042 \times 2^7 = 0.54$. We require $E_{\text{last}} = 0.005$ (i.e. 0.5%), implying that we should choose $h_{\text{last}} = (0.005/0.54)^2 \approx 8 \times 10^{-5}$. We can then expand the mesh spacing away from the singularity by simply multiplying by a suitable factor f, say, where $f > 1$. The simplest way to determine the most appropriate value of f is through numerical experiments. Clearly by choosing a lower level of accuracy, we can set a larger value of h_{last}: for example, repeating this calculation but choosing to aim for 5% accuracy overall, and therefore 2.5% accuracy in the last element gives an estimated $h_{\text{last}} = 0.002$. This approach leads to the mesh spacings,

$$
\begin{aligned}
&h_{n_r-1} = h_{n_r} = h_{\text{last}} \\
&h_{n_r-i} = fh_{n_r-i+1} \qquad \text{for} \quad i = 2,\ldots,n_r \\
&h_{n_r+i} = fh_{n_r+i-1} \qquad \text{for} \quad i = 1,\ldots,n_{r-1} \\
&k_0 \quad = h_{\text{last}} \\
&k_{j+1} \; = fk_j \qquad\qquad \text{for} \quad j = 0,\ldots n_{r-1}
\end{aligned} \tag{24}
$$

An example of a mesh generated in this way is shown in Fig. 5, which was generated using values of $h_{\text{last}} = 8.0 \times 10^{-4}$ and $f = 1.25$.

Table 5 shows the results of these numerical experiments using $h_{\text{last}} = 8.0 \times 10^{-5}$ and 2.0×10^{-3}. As expected, the errors in the final element on these meshes are approximately -0.5% and -2.5%, respectively for all values of the expansion factor f. By choosing the expansion factor appropriately via numerical experiments, we can make use of error cancellation to obtain the total flux to arbitrary accuracy on comparatively coarse meshes. For $h_{\text{last}} = 8.0 \times 10^{-5}$, choosing $f = 1.2473$ gives almost perfect error cancellation and results in a 74×37 mesh (about 2500 nodes in total) with 37 points along the electrode, as shown in Fig. 5. For $h_{\text{last}} = 2.0 \times 10^{-3}$, choosing $f = 1.61$ gives a coarser 26×13 mesh (338 nodes in total) with just 13 points along the electrode. The distribution of the error over the electrode surface when solving on the finer mesh is shown by the dashed line in Fig. 4, and it can be seen that, other than in the last element, the error is now smoothly distributed over the entire electrode surface.

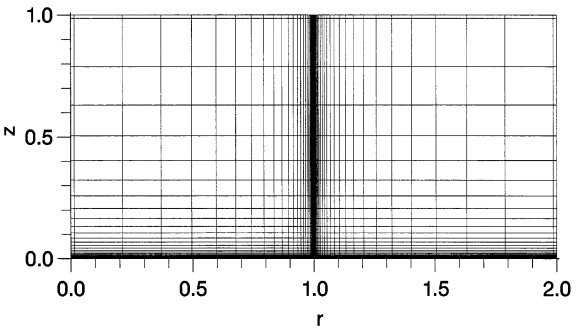

Fig. 5. The refined mesh obtained using values of $h_{\text{last}} = 8.0 \times 10^{-5}$ and $f = 1.25$ in Eq. (24). The mesh has a total of 74 points in the redirection and 37 in the z-direction, with 37 points covering the electrode surface.

4.5. Effect of the far field boundary condition

Throughout the above derivations we have restricted the solution region to the finite region $[0, 2] \times [0, 1]$, using the analytic solution of Eq. (6) as the boundary condition on the far-field boundary. This solution region is large enough to contain the diffusion processes up to intermediate times for the time-dependent problems considered in the accompanying papers. However, for many problems we will be interested in solving for longer times and near-steady-state simulation. In these cases, a much larger solution region will be used and the discretisation at large distances from the electrode will be comparatively course, introducing additional numerical errors. We can estimate the likely magnitude and direction of these errors quite simply by solving the steady-state problem on a larger region. We have done this using the finer of our two meshes with $h_{\text{last}} = 8.0 \times 10^{-5}$, choosing $f = 1.25$. Extending the solution region to $[0, 3] \times [0, 2]$ gave a non-dimensional flux of 1.0020, and to $[0, 6] \times [0, 5]$ gave a flux of 1.0045, so that for very long times we might expect a slight overestimation of the flux using this mesh. Since, in the accompanying papers, we will use the same mesh to solve a very wide variety of problems ranging from very short times to near-steady-state, in Table 6 we have derived a mesh which again uses a value $h_{\text{last}} = 8.0 \times 10^{-5}$, but uses an expansion factor of $f = 1.175$. These mesh parameters provide a good compromise between very short and very long times, being accurate for the steady-state problem to better than 0.25% for a solution region ranging in size from $[0, 2] \times [0, 1]$ up to $[0, 100] \times [0, 100]$. In the accompanying papers it is this mesh which is used to solve problems in chronoamperometry

Table 5
The results of refinement strategy 3

h_{last}	f	$n \times m$	E_{inner}	E_{last}	Flux (Ψ)
8.0×10^{-5}	2.0	28×14	+0.0396	−0.0047	1.0349
8.0×10^{-5}	1.5	44×22	+0.150	−0.0048	1.0102
8.0×10^{-5}	1.25	74×37	+0.0051	−0.0048	1.0003
8.0×10^{-5}	1.2473	74×37	+0.00485	−0.00483	1.00001
8.0×10^{-5}	1.20	86×43	+0.0034	+0.0048	0.9986
2.0×10^{-3}	2.0	18×9	+0.0482	−0.0235	1.025
2.0×10^{-3}	1.5	28×14	+0.0157	−0.0240	0.9916
2.0×10^{-3}	1.6	26×13	+0.0223	−0.0239	0.9984
2.0×10^{-3}	1.61	26×13	+0.0238	−0.0238	0.9999

We first choose the minimum mesh spacing h_{last} and then determine the appropriate expansion factor f by numerical experiment. The overall mesh size is then determined automatically.

and sweep voltammetry across a wide range of parameter values of interest.

4.6. Computing

All programs used to generate results quoted in this paper are written in standard Fortran77 and were run on a Sun Workstation (Spare Ultra 30) which has a 300 MHz processor. The speed of computation is therefore slightly faster than a top-of-the-range PC with a Pentium processor. The CPU time to solve the largest problem quoted (the 125×77 mesh in Table 6) is less than 1 s on this machine. All codes are available from the author on request.

5. Discussion

By investigating in detail the numerical simulation of the flux in steady-state diffusion to a microdisc electrode, we have been able to demonstrate the precise nature of the error over the electrode surface for a variety of mesh refinement strategies. In particular we have demonstrated that it would require approximately 30 million mesh points to obtain acceptable (1%) accuracy using a standard square mesh, due to the polluting effects of the boundary singularity at the electrode edge. We have used the information gained from the investigation to show how to derive a comparatively coarse mesh such as that shown in Fig. 5 on which it is possible, thanks to error cancelling, to obtain the simulated flux to any desired degree of accuracy for the steady-state problem.

Table 6
The effects of altering the position of the far-field boundary

r_{max}, z_{max}	h_{last}	f	$n \times m$	Flux (Ψ)
2.0, 1.0	8.0×10^{-5}	1.175	100×52	0.99795
6.0, 5.0	8.0×10^{-5}	1.175	106×58	1.0002
11.0, 10.0	8.0×10^{-5}	1.175	110×62	1.0010
101.0, 100.0	8.0×10^{-5}	1.175	125×77	1.0025

By choosing $f = 1.175$ we can obtain good accuracy in the calculated flux for regions suitable for a wide range of time-dependent problems.

The final mesh derived uses an expansion factor $f = 1.175$, and a minimum mesh spacing of $h_{last} = 8.0 \times 10^{-5}$, and is designed to yield fast and accurate numerical solutions to other electrochemical problems of interest for which we have no closed form analytic solution. In the accompanying papers we will show that this mesh is ideally suited to the solution of both chronoamperometry [28] and linear sweep voltammetry [29] at a microdisc electrode, allowing the solution of these problems to acceptable accuracy with minimal computing demands.

5.1. Previous work

The results described in this paper also suggest explanations for some of the difficulties experienced by previous authors in using mesh refinement for micro electrode simulations. Heinze and Storzbach [16] used an expanding mesh away from the electrode surface but a constant mesh spacing along the electrode, and their method would therefore not compensate at all for the errors due to the singularity. Taylor et al. [10] used a coordinate transformation dependent on three parameters (doing the same job as f and h_{last} in this paper) to obtain a refined mesh that is quite similar in some respects to that derived in this paper. However, these authors did not consider any error analysis for their method, and it was therefore unclear how to choose an optimal set of parameters. In terms of the work described here, these authors had obtained by numerical experiment a set of mesh parameters which

achieved reasonable error balance, but by adjusting these parameters slightly they could either under, or over estimate the current, just as we have shown in Table 5. It should therefore be possible to derive an optimal set of parameters for Taylor et al.'s method by considering the solution of the steady-state problem in the same way as that described in this paper. In the case of Galceran et al. [9] for the FEM, these authors acknowledge that they simply have not refined their mesh sufficiently to overcome the inaccuracy due to the boundary singularity. In the case of the more recent FEM work of Ferrigno et al. [6], the authors report the much more serious problem of divergence of the simulated flux with mesh refinement. Although these authors do not give exact details of the refinement strategy that they use (they make use of a commercial software package), it is clear from their description that they have refined to a very high degree in a local domain very close to the singularity, but used a very coarse mesh in the 'bulk region'. It therefore seems likely that an effect similar to that described earlier in Section 4.5 is taking place: as the authors have refined their mesh close to the singularity they have removed its effect (a negative error), but the very coarse mesh away from the singularity still gives large (positive) truncation errors, so that as the mesh is refined around the singularity the error balance is destroyed and the simulated flux appears to diverge (fig. 6 of [6]).

Acknowledgements

The author is pleased to acknowledge the financial support of the Wellcome Trust in the form of a Biomathematical Training Fellowship, and a Career Development Fellowship from the Medical Research Council which has allowed him to undertake this research. He also wishes to thank the referee of these three papers for his detailed and helpful comments which have greatly improved the final drafts of the papers.

Appendix A. Derivation of the generalised second order approximations

A.1. Interior nodes

The finite difference approximations to the partial derivatives on a general rectangular mesh can be derived straightforwardly using the Taylor series expansion. Referring to Fig. 1, this gives in the v-direction at interior points

$$u(r-h_{i-1}) = u(r) - h_{i-1}u_r(r) + \frac{h_{i-1}^2}{2!}u_{rr}(r) - \frac{h_{i-1}^3}{3!}u_{rrr}(r) + \dots$$

$$u(r+h_i) = u(r) + h_i u_r(r) + \frac{h_i^2}{2!}u_{rr}(r) + \frac{h_i^3}{3!}u_{rrr}(r) + \dots \quad (25)$$

Eliminating u_{rr} from these equations we obtain the general central difference approximation to u_r as

$$u_r(r) \approx \frac{h_{i-1}^2 u(r+h_i) + (h_i^2 - h_{i-1}^2)u(r) - h_i^2 u(r-h_{i-1})}{h_{i-1}h_i(h_{i-1}+h_i)} \quad (26)$$

and similarly eliminating u_r from these equations we obtain the general central difference approximation to u_{rr} as

$$u_{rr}(r) \approx \frac{2(h_{i-1}u(r+h_i) - (h_i + h_{i-1})u(r) + h_i u(r-h_{i-1}))}{h_{i-1}h_i(h_{i-1}+h_i)} \quad (27)$$

and similarly for z.

A.2. Boundary nodes

To calculate the flux to the electrode and to impose the Neumann condition along the rest of the r-axis, we require a one sided second order finite difference for u_z. This can be found by eliminating u_{zz} from the following equations to give

$$u(k_1) = u(0) + k_0 u_z(0) \frac{k_0^2}{2!}u_{zz}(0) + \frac{k_0^3}{3!}u_{zzz}(0) + \dots$$

$$u(k_0+k_1) = u(0) + (k_0+k_1)u_z(0) + \frac{(k_0+k_1)^2}{2!}u_{zz}(0) + \frac{(k_0+k_1)^3}{3!}u_{zzz}(0) + \dots \quad (28)$$

to give

$$u_z(0) \approx -\frac{k_0^2 u(k_0+k_1) - (k_0+k_1)^2 u(k_0) - (k_1^2 + 2k_0k_1)u(0)}{k_0k_1(k_0+k_1)} \quad (29)$$

References

[1] D.J. Gavaghan, J. Electroanal. Chem. 420 (1997) 147.
[2] R.G. Compton, R.A.W. Dryfe, R.G. Wellington, J. Hirst, J. Electroanal. Chem. 383 (1995) 13.
[3] J.A. Alden, R.G. Compton, J. Electroanal. Chem. 402 (1996) 1.
[4] H. Reller, E. Kirowa-Eisner, E. Gileadi, J. Electroanal. Chem. 138 (1982) 65.
[5] D. Shoup, A. Szabo, J. Electroanal. Chem. 160 (1984) 19.

[6] R. Ferrigno, P.F. Brevet, H.H. Girault, Electrochim. Acta 42 (1997) 1895.
[7] J. Crank, R.M. Furzeland, J. Inst. Maths Applic. 20 (1977) 355.
[8] D.J. Gavaghan, J.S. Rollett, J. Electroanal. Chem. 295 (1990) 1.
[9] J. Galceran, D.J. Gavaghan, J.S. Rollett, J. Electroanal. Chem. 394 (1995) 17.
[10] G. Taylor, H.H. Girault, J. McAleer, J. Electroanal. Chem. 293 (1990) 19.
[11] A.C. Michael, R.M. Wightman, C.A. Amatore, J. Electroanal. Chem. 267 (1989) 33.
[12] I. Lavagnini, P. Pastore, R Magno, C.A. Amatore, J. Electroanal. Chem. 316 (1991) 37.
[13] C.A. Amatore, B. Fossett, J. Electroanal. Chem. 328 (1992) 21.
[14] M.W. Verbrugge, D.R. Baker, J. Phys. Chem. 96 (1992) 4572.
[15] N.T.S. Evans, A.R. Gourlay, J. Inst. Maths. Applics. 19 (1977) 239.
[16] J. Heinze, M. Storzbach, Ber. Bunsenges. Phys. Chem. 90 (1986) 1043.
[17] K. Aoki, J. Osteryoung, J. Electroanal. Chem. 122 (1981) 19.
[18] K.B. Oldham, J. Electroanal. Chem. 122 (1981) 1.
[19] K.B. Oldham, J. Electroanal. Chem. 260 (1989) 461.
[20] A.M. Bond, K.B. Oldham, C.G. Zoski, J. Electroanal. Chem. 245 (1988) 71.
[21] M. Fleischmann, S. Pons, J. Electroanal. Chem. 250 (1988) 257.
[22] M. Fleischmann, J. Daschbach, S. Pons, J. Electroanal. Chem. 250 (1988) 269.
[23] D.K. Cope, D.E. Tallman, J. Electroanal. Chem. 373 (1994) 53.
[24] Y. Saito, Rev. Polarogr. (Jpn) 15 (1968) 177.
[25] D.J. Gavaghan, J.S. Rollett, C.E.W. Hahn, J. Electroanal. Chem. 325 (1992) 23.
[26] L. Sutton, D.J. Gavaghan, C.E.W. Hahn, J. Electroanal. Chem. 408 (1996) 21.
[27] J. Galceran, J. Salvador, J. Puy, J. Cecilia, D.J. Gavaghan, J. Electroanal. Chem. 440 (1997) 1.
[28] D.J. Gavaghan, J. Electroanal. Chem. 456 (1998) 13.
[29] D.J. Gavaghan, J. Electroanal. Chem. 456 (1998) 25.
[30] K.W. Morton, D.F. Mayers, Numerical Solution of Partial Differential Equations, Cambridge University Press, Cambridge, 1994.
[31] R.V. Southwell, Proc. Roy. Soc. 151 (1935) 56.
[32] The NAG Fortran Library Manual-Mark 14, The Numerical Algorithms Group Limited, (1990).
[33] D. Britz, Digital Simulation in Electrochemistry, 2nd ed., Springer, Heidelberg, 1988.